New Journal of Physics
The open access journal at the forefront of physics

Deutsche Physikalische Gesellschaft DPG IOP Institute of Physics

PAPER • OPEN ACCESS

High-efficiency triple-resonant inelastic light scattering in planar optomagnonic cavities

New Journal of Physics
The open access journal at the forefront of physics

Deutsche Physikalische Gesellschaft DPG
IOP Institute of Physics

Published in partnership with: Deutsche Physikalische Gesellschaft and the Institute of Physics

OPEN ACCESS

RECEIVED
14 May 2019

REVISED
5 August 2019

ACCEPTED FOR PUBLICATION
13 August 2019

PUBLISHED
4 September 2019

PAPER

High-efficiency triple-resonant inelastic light scattering in planar optomagnonic cavities

Petros Andreas Pantazopoulos, Kosmas L Tsakmakidis, Evangelos Almpanis, Grigorios P Zouros and Nikolaos Stefanou

Section of Solid State Physics, National and Kapodistrian University of Athens, Panepistimioupolis, GR-157 84 Athens, Greece

E-mail: pepantaz@phys.uoa.gr

Keywords: optomagnonic cavity, Voigt geometry, magnetostatic spin waves, inelastic light scattering, time Floquet method

Abstract

Optomagnonic cavities have recently been emerging as promising candidates for implementing coherent photon-magnon interactions, for applications in quantum memories and devices, and next generation quantum networks. A key challenge in the design of such cavities is the attainment of high magnon-mediated optical-to-optical conversion efficiencies, which could, e.g., be exploited for efficient optical interfacing of superconducting qubits, as well as the practicality of the final designs, which ideally should be planar and amenable to on-chip integration. Here, on the basis of a novel time-Floquet scattering-matrix approach, we report on the design and optimization of a planar, multilayer optomagnonic cavity, incorporating a cerium-substituted yttrium iron garnet thin film, magnetized in-plane, and operating in the triple-resonant inelastic light scattering regime. This architecture allows for magnon-mediated optical-to-optical conversion efficiencies of about 5% under realistic conditions, which is orders of magnitude higher than that attained in alternative optomagnonic designs. Our results suggest a viable way forward for realizing practical information inter-conversion, with high efficiencies, between microwaves, strongly coupled to magnons, and optical photons, as well as a platform for fundamental studies of classical and quantum dynamics in magnetic solids and for the implementation of futuristic quantum devices.

1. Introduction

A key difficulty for achieving efficient magnon-assisted microwave-to-optical transduction is the inherently weak coupling between optical photons and microwave-triggered magnonic excitations, termed optomagnonic interaction, hindering among others the long-awaited optical interfacing of superconducting qubits [1–5]. To this end, judiciously designed dielectric structures, which include magnetic materials, capable of simultaneously confining light (optical photons) and spin waves (magnons) in the same region of space, so-called optomagnonic cavities, are currently being actively studied as they might potentially form ideal hosts for attaining increased optomagnonic interactions.

The optomagnonic interaction is expected to be large when the so-called triple-resonance condition is met, i.e. when the frequency of a cavity magnon matches the frequency difference between two resonant optical modes, which translates to an optimal optical-photon sideband generation through the respective absorption or emission of a magnon. This implies that the cavity must support two well-resolved optical resonances (in the hundred terahertz range) separated by a few gigahertz, which requires quality factors at least of the order of 10^5, as schematically depicted in figure 1.

A (sub)millimeter-sized sphere, made of a low-loss dielectric magnetic material, constitutes a simple realization of an optomagnonic cavity. The sphere supports densely spaced long-lifetime optical whispering gallery modes (WGM) [6–10], and infrared incident light evanescently coupled to these modes can be scattered by a uniformly precessing (so-called Kittel) spin wave to a neighboring optical WGM. In the aforementioned cases, the coupling between WGM and Kittel magnons is rather inefficient, resulting in measured magnon-

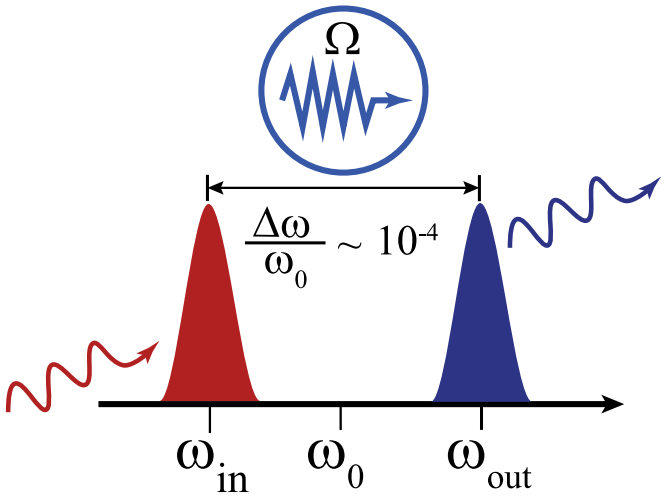

Figure 1. Schematic of inelastic light scattering through magnon absorption in an optomagnonic cavity. The frequency of a cavity magnon, Ω, matches a photon transition between two resonant optical modes: $\Omega = \Delta\omega \equiv \omega_{\rm out} - \omega_{\rm in}$ (triple-resonance condition).

mediated optical-to-optical conversion (optical sideband generation) efficiencies that do not exceed the order of 10^{-6} [6, 7]. In the prospect of achieving smaller modal volumes and larger spatial overlap between the interacting fields, higher-order magnetostatic modes [11–13], magnetically-split optical Mie resonances in small spheres [14], as well as particles of different shapes [15] have been proposed. However, these proposals currently face appreciable challenges in the fabrication of high-quality particles and/or the efficient excitation of the spin waves.

A promising alternative design of optomagnonic cavities is based on *planar* geometries, which can exhibit even stronger conversion efficiencies, while at the same time allowing integration into a hybrid opto-microwave chip using modern nanofabrication methods. In a recent work on a planar-waveguide optomagnonic architecture, using a lossless bismuth-substituted yttrium iron garnet (Bi:YIG) film as active material, optical-to-optical conversion efficiencies ranging from 10^{-5} to almost 10^{-2} (depending on the thickness of the film) were predicted [16]. However, since light is guided inside Bi:YIG, the introduction of realistic dissipative losses would result in significant decrease of the efficiency. To this end, optomagnonic cavities formed in a magnetic dielectric film bounded by two mirrors [17–19], or in a defect layer in a dual photonic-magnonic periodic layered structure [20], have also been investigated. However, the studies reported so far refer to the Faraday configuration, with out-of-plane magnetized films, where it is challenging to obtain two optical resonances in the required close proximity to each other.

In this work we show that, by using in-plane magnetized films in the so-called Voigt configuration, we can overcome the afore-described shortcomings of previous schemes and design efficient optomagnonic cavities operating in the triple-resonance regime. In section 2 we describe the statically magnetized structure and discuss its optical response. In section 3 we summarize our recently developed fully dynamic time-Floquet method for layered optomagnonic structures [19] and in section 4 we present details of our attained numerical results. The last section concludes the article.

2. Structure design

We propose a simple design of planar optomagnonic cavity, simultaneously confining light and spin waves in the same subwavelength region of space. It consists of an iron garnet thin film bounded symmetrically by two lossless, dielectric Bragg mirrors, in air, as schematically illustrated in figure 2(a).

Iron garnets are ferrimagnetic materials exhibiting important functionalities for bulk and thin-film device applications that require magnetic insulators, owing to their unique physical properties such as high optical transparency in a wide range of wavelengths, high Curie temperature, ultra-low spin-wave damping, and strong magneto-optical coupling [21]. In our work, we consider cerium-substituted yttrium iron garnet (Ce:YIG) which, at the telecom wavelength of 1.5 μm, has a relative electric permittivity $\epsilon = 5.10 + {\rm i}10^{-4}$ and a Faraday coefficient $f = -0.01$ [22], while its relative magnetic permeability equals unity. The Ce:YIG film extends from $z = -d/2$ to $z = d/2$ and is magnetically saturated to M_0 by an in-plane bias magnetic field H_0 oriented, say, along the x direction. Therefore, the corresponding relative electric permittivity tensor, neglecting the small Cotton–Mouton contributions, is of the form [23]

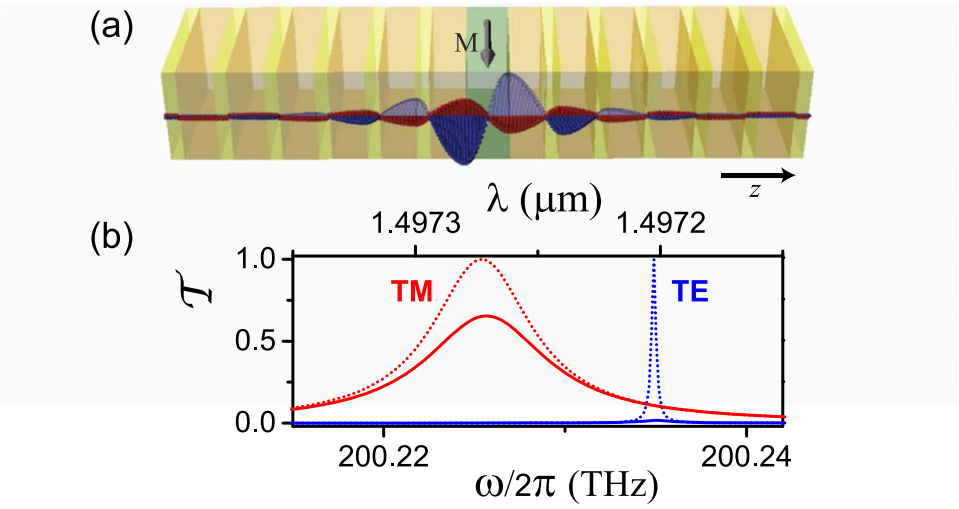

Figure 2. (a) Schematic view of the optomagnonic cavity under study. It is formed by a 350 nm thick Ce:YIG film magnetized in-plane (along the x direction), bounded symmetrically by two Bragg mirrors, each consisting of 6 periods of alternating SiO_2 and Si layers of thickness 290 nm and 110 nm, respectively, grown along the z direction. For light incident with $q_y = 3\ \mu\text{m}^{-1}$, the cavity supports two localized resonant modes, one of TM and one of TE polarization, manifested in the corresponding transmission spectrum shown in (b), with the dotted and solid curves referring to the lossless and lossy structure, respectively. A snapshot of the associated electric field profiles along the z direction in the lossless case is illustrated in (a).

$$\boldsymbol{\epsilon} = \begin{pmatrix} \epsilon & 0 & 0 \\ 0 & \epsilon & if \\ 0 & -if & \epsilon \end{pmatrix}. \tag{1}$$

We consider the Voigt geometry with light propagating in the y–z plane. The structure in this geometry, with the magnetic field parallel to the surface and also perpendicular to the propagation direction, remains invariant under reflection with respect to the plane of incidence. Consequently, contrary to the Faraday configuration studied in our previous work [18–20], the transverse magnetic (TM) and transverse electric (TE) polarization modes, i.e. modes with the electric field oscillating in and normal to the plane of incidence, respectively, are eigenmodes of the system. Interestingly, in the chosen geometry, the magnetic film behaves as isotropic, with permittivity $\epsilon - f^2/\epsilon$ and ϵ for TM- and TE-polarized waves, respectively. In other words, only TM-polarized light is affected by the (magnetic) polarization field.

Each Bragg mirror consists of an alternate sequence of six SiO_2 and six Si quarter-wave layers, i.e. $d_{\text{m}}\sqrt{(2\pi n_{\text{m}}/\lambda)^2 - q_y^2} = \pi/2$, where d_{m} (m: SiO_2 or m: Si) is the layer thickness and n_{m} the corresponding refractive index ($n_{SiO_2} = 1.47$ and $n_{\text{Si}} = 3.5$) at the operation wavelength $\lambda \approx 1.5\ \mu$m [24, 25]. Due to translation invariance parallel to the x–y plane, the in-plane component of the wave vector, $q_y = 2\pi \sin\theta/\lambda$, where θ is the angle of incidence, remains constant. Taking, for instance, $q_y = 3\ \mu\text{m}^{-1}$, which corresponds to an angle of incidence of about 45°, we obtain $d_{SiO_2} = 290$ nm and $d_{\text{Si}} = 110$ nm. Accordingly, we choose a thickness $d = 350$ nm for the Ce:YIG film to satisfy the half-wave condition that corresponds to transmission maxima.

This design provides two (one TM and one TE) high-quality-factor resonances within the lowest Bragg gap, at a wavelength of about 1.5 μm, separated by a frequency difference $\Delta\omega/2\pi = 9.5$ GHz that matches the frequency of magnetostatic spin waves [21, 23]. These resonant modes are strongly localized in the region of the Ce:YIG film, which can be considered as a defect in the periodic stacking sequence of the Bragg mirrors. Absorption losses reduce the transmittance peak. In particular, the long-lifetime TE resonance is strongly suppressed in the presence of dissipative losses, as shown by the solid blue line in figure 2(b).

It should be pointed out that the position and width of the optical resonances can be tailored at will by appropriate selection of the materials, and by properly adjusting the geometric parameters of the structure and the angle of incidence. Such one-dimensional statically magnetized, so-called magnetophotonic, structures have long been investigated either in the Faraday [26] or in the Voigt [27] configuration.

3. Theory for layered optomagnonic structures

The magnetic Ce:YIG film supports magnetostatic spin waves where the magnetization precesses in-phase, elliptically, throughout the film (uniform precession mode) with angular frequency $\Omega = \sqrt{\Omega_H(\Omega_H + \Omega_M)}$,

where $\Omega_H = \gamma\mu_0 H_0$ and $\Omega_M = \gamma\mu_0 M_0$, γ being the gyromagnetic ratio and μ_0 the magnetic permeability of vacuum [23]. The corresponding magnetization field profile is given by

$$\mathbf{M}(\mathbf{r},\, t)/M_0 = \hat{\mathbf{x}} + \eta A_y \sin(\Omega t)\hat{\mathbf{y}} + \eta A_z \cos(\Omega t)\hat{\mathbf{z}}, \tag{2}$$

where $A_y = \sqrt{(\Omega_H + \Omega_M)/(2\Omega_H + \Omega_M)}$, $A_z = \sqrt{\Omega_H/(2\Omega_H + \Omega_M)}$, and η is an amplitude factor that defines the magnetization precession angle.

Under the action of the spin wave, the magnetic film and, consequently, the entire structure can be looked upon as a periodically driven system because the magnetization field, given by equation (2), induces a temporal perturbation [18]

$$\delta\boldsymbol{\epsilon}\,(t) = \frac{1}{2}[\delta\boldsymbol{\epsilon}\,\exp(-\mathrm{i}\Omega t) + \delta\boldsymbol{\epsilon}^{\dagger}\exp(\mathrm{i}\Omega t)] \tag{3}$$

in the permittivity tensor of the statically magnetized material, where

$$\delta\boldsymbol{\epsilon} = f\eta\begin{pmatrix} 0 & \mathrm{i}A_z & A_y \\ -\mathrm{i}A_z & 0 & 0 \\ -A_y & 0 & 0 \end{pmatrix}. \tag{4}$$

The periodically driven system can be studied using our recently developed time-Floquet scattering-matrix method, which is a powerful tool for studying inelastic light scattering by planar structures that comprise periodically time-varying media, such as the one considered in the present work, without using any adjustable parameters. The method goes beyond phenomenological modeling [6–8], and rigorously provides the optical-to-optical conversion efficiency in a straightforward manner since it evaluates the intensity of all (elastically and inelastically) transmitted and reflected light beams associated with all magnon absorption and emission processes. In this respect, contrary to other approaches [10, 16], it is not restricted to the linear-response regime and is correct to any order in perturbation theory. The essentials of the time-Floquet scattering-matrix method are summarized below.

The solutions of the Maxwell equations for the dynamic structure under consideration are Floquet modes $\mathbf{F}(\mathbf{r},\, t) = \mathrm{Re}\{\boldsymbol{\mathcal{F}}(\mathbf{r},\, t)\exp(-\mathrm{i}\omega t)\}$, with $\boldsymbol{\mathcal{F}}(\mathbf{r},\, t + T) = \boldsymbol{\mathcal{F}}(\mathbf{r},\, t)$, $T = 2\pi/\Omega$, where by $\mathbf{F}$ we denote electric field, electric displacement, magnetic field, and magnetic induction, while ω is the Floquet quasi-frequency, similarly to the Floquet quasi-momentum (or else the Bloch wave vector) when there is spatial periodicity [28, 29]. Seeking Floquet modes in the form of plane waves with given q_y and expanding all time-periodic quantities into truncated Fourier series in the basis of complex exponential functions $\exp(\mathrm{i}n\Omega t)$, $n = -N,\, -N + 1,\, \ldots,\, N$, leads to an eigenvalue-eigenvector equation, which has $4(2N + 1)$ physically acceptable solutions [19]. We characterize them by the following indices: $s = +(-)$ that denotes waves propagating or decaying in the positive (negative) z direction, $p = 1, 2$ that indicates the two eigen-polarizations, and $\nu = -N,\, -N + 1, \cdots,\, N$ which labels the different eigenmodes. These eigenmodes are polychromatic waves, each composed of $2N + 1$ monochromatic components of angular frequency $\omega - n\Omega$, $n = -N$, $-N + 1, \ldots, N$ [19]. We note that, in a static homogeneous medium, the corresponding eigenmodes of the electromagnetic (EM) field are monochromatic waves characterized by the indices s, p, and n.

Scattering of an eigenmode occurs at an interface between two different homogeneous media. We assume that the interface is perpendicular to the z axis, which is directed from left to right, at $z = 0$. For such a planar interface between a static and a time-periodic medium, the relative complex amplitudes of the transmitted (reflected) waves, denoted by $Q^{21}_{p\nu;p'n'}$ ($Q^{11}_{pn;p'n'}$) for incidence in the forward direction or $Q^{12}_{pn;p'\nu'}$ ($Q^{22}_{p\nu;p'\nu'}$) for incidence in the backward direction in the configuration shown in figure 3, are obtained in the manner described in [19]. Primed indices refer to the incident wave. For an interface between two static homogeneous media, the Q matrices relate monochromatic waves and are diagonal in n, which reflects frequency conservation. We note that, in order to evaluate the scattering properties of layered optomagnonic structures in a straightforward manner, the waves on each side of a given interface are expressed around different points, at a distance $-\mathbf{d}_1$ and $\mathbf{d}_2$ from the center of the interface (see figure 3), so that all backward and forward propagating or evanescent waves in the region between two consecutive interfaces refer to the same (arbitrary) origin. Of course, because of translation invariance parallel to the x–y plane, the choice of the x–y components of $\mathbf{d}_1$ and $\mathbf{d}_2$ are immaterial; thus, for simplicity, we choose $\mathbf{d}_1$ and $\mathbf{d}_2$ along the z direction.

The transmission and reflection matrices of a pair of consecutive interfaces, i and $i + 1$, are obtained by properly combining those of the two interfaces so as to describe multiple scattering to any order. This leads to the following expressions after summing up the infinite geometric series involved, as schematically illustrated in figure 3, i.e.

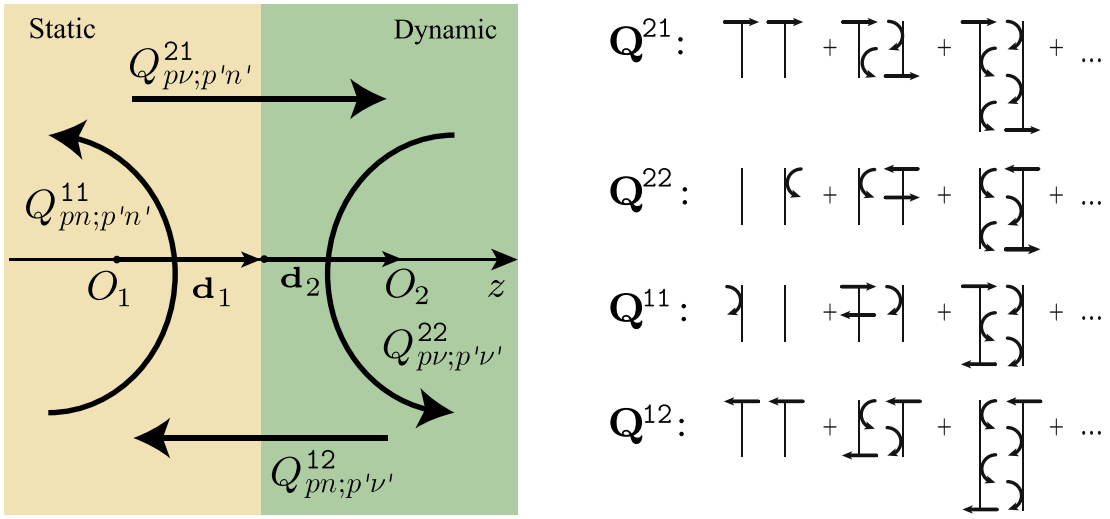

Figure 3. Left-hand diagram: Transmission and reflection matrices for a planar interface between a static and a dynamic medium, defined with respect to appropriate origins, O_1 and O_2, at distances $-\mathbf{d}_1$ and $\mathbf{d}_2$ from a center at the interface, respectively. Right-hand diagram: The transmission and reflection matrices of two consecutive interfaces are evaluated by summing up all relevant multiple-scattering processes.

$$\begin{aligned}
\mathbf{Q}^{21}(i,\,i+1) &= \mathbf{Q}^{21}(i+1)[\mathbf{I}-\mathbf{Q}^{22}(i)\mathbf{Q}^{11}(i+1)]^{-1}\mathbf{Q}^{21}(i)\\
\mathbf{Q}^{22}(i,\,i+1) &= \mathbf{Q}^{22}(i+1)+\mathbf{Q}^{21}(i+1)\mathbf{Q}^{22}(i)[\mathbf{I}-\mathbf{Q}^{11}(i+1)\mathbf{Q}^{22}(i)]^{-1}\mathbf{Q}^{12}(i+1)\\
\mathbf{Q}^{11}(i,\,i+1) &= \mathbf{Q}^{11}(i)+\mathbf{Q}^{12}(i)\mathbf{Q}^{11}(i+1)[\mathbf{I}-\mathbf{Q}^{22}(i)\mathbf{Q}^{11}(i+1)]^{-1}\mathbf{Q}^{21}(i)\\
\mathbf{Q}^{12}(i,\,i+1) &= \mathbf{Q}^{12}(i)[\mathbf{I}-\mathbf{Q}^{11}(i+1)\mathbf{Q}^{22}(i)]^{-1}\mathbf{Q}^{12}(i+1).
\end{aligned} \tag{5}$$

It should be noted that the waves on the left (right) of the pair of interfaces are referred to an origin at a distance $-\mathbf{d}_1(i)$ [$\mathbf{d}_2(i+1)$] from the center of the ith [$(i+1)$th] interface. We also recall that, though the choice of $\mathbf{d}_1$ and $\mathbf{d}_2$ associated to each interface is to a certain degree arbitrary, it must be such that $d_{2z}(i)+d_{1z}(i+1)$ equals the thickness of the layer between the ith and $(i+1)$th interfaces. It is obvious that one can repeat the above process to obtain the transmission and reflection matrices $\mathbf{Q}$ of three consecutive interfaces, by combining those of the pair of the first interfaces with those of the third interface, and so on, by properly combining the Q matrices of component units, one can obtain the Q matrices of a slab which comprises any finite number of interfaces [28, 29]. This method applies to an arbitrary slab which comprises periodically time-varying layers, provided that all dynamic media have the same temporal periodicity. It is then straightforward to calculate the transmittance, $\mathcal{T}$, and reflectance, $\mathcal{R}$, of the slab as the ratio of the transmitted and reflected, respectively, energy flux to the energy flux associated with the incident wave. $\mathcal{T}$ and $\mathcal{R}$ are given by the sum of the corresponding quantities over all scattering channels (p,n): $\mathcal{T}=\sum_{p,n}\mathcal{T}_{pn}$ and $\mathcal{R}=\sum_{p,n}\mathcal{R}_{pn}$. It is worth noting that, because of the time variation of the permittivity tensor, the EM energy is not conserved even in the absence of dissipative (thermal) losses. In this case, $\mathcal{A}=1-\mathcal{T}-\mathcal{R}>0(<0)$ means energy transfer from (to) the EM to (from) the spin-wave field.

We note that, here, we employ the scattering-matrix method, as we formulated it for photonic crystals [28–30] following the mathematical concepts and notation of low-energy electron diffraction theory [31]. Alternatively, one could adopt the transfer-matrix method [32–34]. This simply reverts to a product of matrices associated with the individual scattering units, allowing an efficient parallel numerical evaluation, while the scattering-matrix approach yields a recursion (see equation (5)) that has to be evaluated step by step. However, despite its advantages, the transfer-matrix method may suffer from numerical instabilities [35], which are not encountered in the scattering-matrix method [36].

We close this section by pointing out a useful polarization selection rule, which can be readily derived in the linear-response approximation. To first order, the coupling strength associated to the photon-magnon scattering is proportional to the overlap integral $G=\langle\text{out}|\,\delta\epsilon\,|\text{in}\rangle$, where $\langle\mathbf{r}t|\text{in}\rangle=\mathbf{E}^{\text{in}}(z)\exp[\text{i}(\mathbf{q}_\parallel\cdot\mathbf{r}-\omega t)]$ and $\langle\text{out}|\mathbf{r}'t'\rangle=\mathbf{E}^{\text{out}\star}(z)\exp[-\text{i}(\mathbf{q}'_\parallel\cdot\mathbf{r}-\omega' t)]$ denote appropriate incoming and outgoing monochromatic time-harmonic waves in the static magnetic layered structure. Using equation (3) we obtain

$$G=4\pi^3 f\eta\delta(\mathbf{q}_\parallel-\mathbf{q}'_\parallel)[\delta(\omega-\omega'-\Omega)g_-+\delta(\omega-\omega'+\Omega)g_+], \tag{6}$$

where $g_\pm=\mathbf{u}_\pm\cdot\int\text{d}z[\mathbf{E}^{\text{out}\star}(z)\times\mathbf{E}^{\text{in}}(z)]$, with $\mathbf{u}_\pm=\mp A_y\hat{\mathbf{y}}+\text{i}A_z\hat{\mathbf{z}}$. The delta functions in equation (6) express conservation of in-plane momentum and energy in inelastic light scattering processes that involve emission and absorption of one magnon by a photon, as expected in the linear regime. Obviously, the amplitude

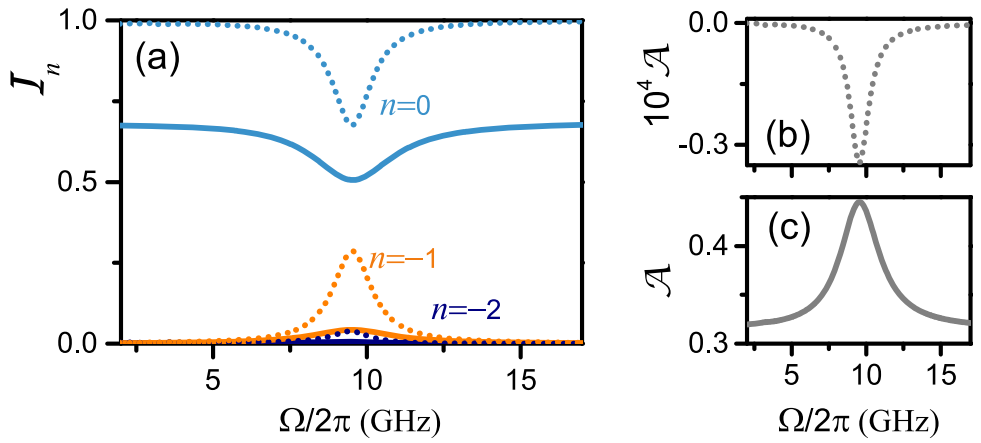

Figure 4. The structure of figure 2(a), under continuous excitation of a uniform precession spin-wave mode of angular frequency Ω with a relative amplitude $\eta = 0.06$, is illuminated from the left by TM-polarized light with $q_y = 3\ \mu\text{m}^{-1}$ at the corresponding resonance frequency (see figure 2(b)). Variation of the dominant elastic and inelastic total outgoing light intensities versus the spin-wave frequency (a) and corresponding optical absorption (b) and (c). Dotted and solid curves refer to the lossless and lossy structure, respectively.

of transition between two optical eigenmodes of the same polarization, TM or TE, is identically zero because the corresponding eigenvectors are real. In other words, one-magnon processes change the linear polarization state of a photon.

4. Results and discussion

We now assume continuous excitation of a uniform-precession spin-wave mode in the magnetic film, with a relative amplitude $\eta = 0.06$, which induces a periodic time variation in the corresponding electric permittivity tensor, given by equation (3). The optomagnonic structure is illuminated from the left by TM-polarized light with $q_y = 3\ \mu\text{m}^{-1}$ at the corresponding resonance frequency, which corresponds to an angle of incidence of about 45°. The dynamic optical response of the structure is calculated with sufficient accuracy by considering a cutoff of $N = 5$ in the Fourier series expansions involved in our time-Floquet scattering-matrix method outlined in section 3.

Figure 4(a) shows the total (transmitted plus reflected) intensities, $\mathcal{I}_n = \sum_p(\mathcal{T}_{pn} + \mathcal{R}_{pn})$, as a function of the spin-wave frequency $\Omega/2\pi$. It can be seen that inelastic light scattering is negligible when the allowed final photon states fall within a gap, where the optical density of states is very low, and we essentially have only the elastically scattered beam. On the contrary, when the spin-wave frequency matches the frequency difference $\Delta\omega/2\pi = 9.5$ GHz between the two optical resonances (see figure 2(a)), the triple-resonance condition is fulfilled and one-magnon absorption processes are favored, leading to enhanced intensities of the corresponding ($n = -1$) inelastically transmitted and reflected light beams, with a maximum value of 0.3 if dissipative losses are neglected. In other words, the magnon-mediated optical-to-optical conversion efficiency is as high as 30%. At the same time, the elastically scattered beam intensity is considerably reduced while the other inelastic processes are also resonantly affected, though to a much lesser degree, as shown in figure 4(a) and also in figure 5. We note that the total outgoing inelastically scattered beam intensity is almost equally distributed between the corresponding transmitted and reflected light beams.

Overall, there is an excess number of magnons absorbed, which can be accounted for by our fully dynamic time-Floquet scattering-matrix method [19]. This is manifested as a small negative absorption peak (see figure 4(b)), which clearly indicates a resonant energy transfer from the magnon to the photon field. We note that, despite this net transfer rate of magnons, our description assumes an undamped uniform precession of the magnetization in the Ce:YIG film, i.e. a magnon bath where the number of particles is kept constant.

Considering a saturation magnetization $M_0 = 150$ emu cm^{-3} for Ce:YIG [22], the triple-resonance condition ($\Omega/2\pi = 9.5$ GHz) is achieved with a bias magnetic field $H_0 = 2.5$ kOe. In this case, the cone angle of magnetization precession (elliptical in the chosen configuration) attains a maximum of 2.75°, which is a tolerable value for linear spin waves.

It is interesting to note that the triple-resonance condition can be accomplished by many-magnon absorption processes as well ($m\Omega = \Delta\omega$), provided that the number of magnons, m, is odd in order to change the polarization state of the photon, from TM to TE, as required in our case. We recall that our method of calculation is not restricted to the first-order Born approximation and thus it can describe nonlinear effects that

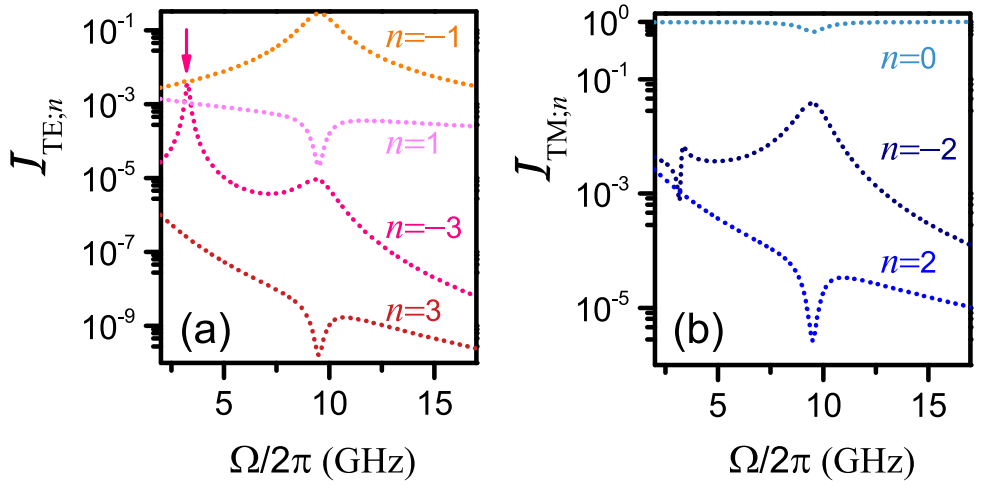

Figure 5. Polarization-converting (a) and polarization-conserving (b) contributions to the spectrum of the figure 4(a). The peak in (a) indicated by the arrow corresponds to the resonant transition when accomplished by absorption of three magnons.

are usually relatively weak. For example, such a three-magnon absorption process is manifested as a peak in the intensity of the $n = -3$ outgoing beam, for $\Omega/2\pi = (\Delta\omega/2\pi)/3 \approx 3.2$ GHz, as pointed out by the arrow in figure 5(a).

As can be seen in figure 4(a), when dissipative losses are taken into account, the elastically scattered beam intensity is uniformly reduced by about 30%, in agreement with the results shown in figure 2(b) for the TM mode. Here, when the triple-resonance condition is satisfied, the corresponding drop in the $n = -1$ beam is considerably larger because of the longer lifetime of the final (TE) state but, nonetheless, the conversion efficiency is still as high as 5% (see solid orange curve in figure 4(a)). We note that, because of the high quality factor of the final (TE) state and the presence of non-negligible losses in this case, we overall obtain resonant optical absorption (see figure 4(c)), instead of gain in the lossless case as shown in figure 4(b).

The obtained magnon-mediated optical-to-optical conversion efficiency of 5% under realistic conditions is larger than that measured in YIG spheres [6, 7], which does not exceed the order of 10^{-6}, and also at least one order of magnitude higher than the theoretically estimated efficiencies in lossless planar-waveguide optomagnonic architectures [16]. The performance of our design can be further improved by carefully engineering high-quality-factor optical modes, which requires the selection of low-loss materials, ensuring also an inherently strong magneto-optical coupling. For example, much higher optical-to-optical conversion efficiencies can be obtained by designing our structure to operate at longer wavelengths where iron garnets exhibit negligible optical losses while maintaining an appreciable Faraday coefficient [22].

It is worth noting that, in our case, the assumption of linear EM response implies that, at given spin-wave power, the intensity of the converted outgoing optical beam is proportional to that of the incident pump light. On the other hand, our calculations show that the ratio of the above intensities, i.e. the optical-to-optical conversion efficiency, increases linearly with the spin-wave power ($\sim\eta^2$) up to $\eta \simeq 0.03$, as expected on the basis of equation (6) for one-magnon absorption mechanisms. For higher values of η the linear-response regime breaks down, indicating the occurrence of multi-magnon exchange processes, while the conversion efficiency continues to increase, though at a smaller rate, and takes the value of 5% at $\eta = 0.06$.

5. Conclusions

To conclude, we have presented a detailed analysis and optimization of a planar optomagnonic structure operating in the triple-resonance regime and allowing for magnon-mediated optical-to-optical conversion efficiencies of the order of 5% (see figure 4(a)) under realistic conditions, mediated by a uniformly precessing spin wave. The outlined time-Floquet multiple-scattering methodology was able to resolve absorption and emission of *multiple* magnons, indicating that under special conditions the attained conversion efficiencies mediated by, e.g. three magnons can be comparable to those mediated by a single magnon (see orange and pink dotted lines in figure 5(a)). We have also found that the absorption or emission of a magnon leads to a change in the polarization of the optical conversion process. An interesting further objective would be to extend the current approach to the full *spatio*-temporal Floquet scattering-matrix methodology, which should allow for investigating, among others, surface Damon–Eshbach and backward volume waves with an in-plane

propagation wavevector that can lead to more exotic physical behavior, such as emergence of a paraxial outgoing scattered beam and bandgap formation.

Acknowledgments

PAP was supported by the General Secretariat for Research and Technology (GSRT) and the Hellenic Foundation for Research and Innovation (HFRI) through a PhD scholarship (No. 906). KLT, EA, and GPZ were supported by HFRI and GSRT under Grant 1819.

ORCID iDs

Petros Andreas Pantazopoulos https://orcid.org/0000-0003-2520-9380
Evangelos Almpanis https://orcid.org/0000-0001-8128-3118
Grigorios P Zouros https://orcid.org/0000-0003-4054-6086
Nikolaos Stefanou https://orcid.org/0000-0003-1264-472X

References

[1] Tabuchi Y, Ishino S, Noguchi A, Ishikawa T, Yamazaki R, Usami K and Nakamura Y 2015 Coherent coupling between a ferromagnetic magnon and a superconducting qubit *Science* **349** 405–8
[2] Hisatomi R, Osada A, Tabuchi Y, Ishikawa T, Noguchi A, Yamazaki R, Usami K and Nakamura Y 2016 Bidirectional conversion between microwave and light via ferromagnetic magnons *Phys. Rev.* B **93** 174427
[3] Lachance-Quirion D, Tabuchi Y, Ishino Y, Noguchi A, Ishikawa T, Yamazaki R and Nakamura Y 2017 Resolving quanta of collective spin excitations in a millimeter-sized ferromagnet *Sci. Adv.* **3** e1603150
[4] Lachance-Quirion D, Tabuchi Y, Gloppe A, Usami K and Nakamura Y 2019 Hybrid quantum systems based on magnonics *Appl. Phys. Express* **12** 070101
[5] Lambert N J, Rueda A, Sedlmeir F and Schwefel H G 2019 Coherent conversion between microwave and optical photons-an overview of physical implementations arXiv:1906.10255
[6] Osada A, Hisatomi R, Noguchi A, Tabuchi Y, Yamazaki R, Usami K, Sadgrove M, Yalla R, Nomura M and Nakamura Y 2016 Cavity optomagnonics with spin–orbit coupled photons *Phys. Rev. Lett.* **116** 223601
[7] Zhang X, Zhu N, Zou C-L and Tang H X 2016 Optomagnonic whispering gallery microresonators *Phys. Rev. Lett.* **117** 123605
[8] Haigh J A, Nunnenkamp A, Ramsay A J and Ferguson A J 2016 Triple-resonant Brillouin light scattering in magneto-optical cavities *Phys. Rev. Lett.* **117** 133602
[9] Viola Kusminskiy S, Tang H X and Marquard F 2016 Coupled spin-light dynamics in cavity optomagnonics *Phys. Rev.* A **94** 033821
[10] Sharma S, Blanter Y M and Bauer G E W 2017 Light scattering by magnons in whispering gallery mode cavities *Phys. Rev.* B **96** 094412
[11] Haigh J A, Lambert N J, Sharma S, Blanter Y M, Bauer G E W and Ramsay A J 2018 Selection rules for cavity-enhanced Brillouin light scattering from magnetostatic modes *Phys. Rev.* B **97** 214423
[12] Osada A, Gloppe A, Hisatomi R, Noguchi A, Yamazaki R, Nomura M, Nakamura Y and Usami K 2018 Brillouin light scattering by magnetic quasivortices in cavity optomagnonics *Phys. Rev. Lett.* **120** 133602
[13] Osada A, Gloppe A, Nakamura Y and Usami K 2018 Orbital angular momentum conservation in Brillouin light scattering within a ferromagnetic sphere *New J. Phys.* **20** 103018
[14] Almpanis E 2018 Dielectric magnetic microparticles as photomagnonic cavities: enhancing the modulation of near-infrared light by spin waves *Phys. Rev.* B **97** 184406
[15] Graf J, Pfeifer H, Marquardt F and Viola Kusminskiy S 2018 Cavity optomagnonics with magnetic textures: coupling a magnetic vortex to light *Phys. Rev.* B **98** 241406(R)
[16] Kostylev M and Stashkevich A A 2019 Proposal for a microwave photon to optical photon converter based on traveling magnons in thin magnetic films *J. Magn. Magn. Mater.* **484** 329–44
[17] Liu T Y, Zhang X F, Tang H X and Flatté M E 2016 Optomagnonics in magnetic solids *Phys. Rev.* B **94** 060405(R)
[18] Pantazopoulos P A, Stefanou N, Almpanis E and Papanikolaou N 2017 Photomagnonic nanocavities for strong light-spin-wave interaction *Phys. Rev.* B **96** 104425
[19] Pantazopoulos P A and Stefanou N 2019 Layered optomagnonic structures: time Floquet scattering-matrix approach *Phys. Rev.* B **99** 144415
[20] Pantazopoulos P A, Papanikolaou N and Stefanou N 2019 Tailoring coupling between light and spin waves with dual photonic-magnonic resonant layered structures *J. Opt.* **21** 015603
[21] Zvezdin A K and Kotov V A 1997 *Modern Magnetooptics and Magnetooptical Materials* (Bristol: Institute of Physics Publishing)
[22] Onbasli M C, Beran L, Zahradník M, Kučera M, Antoš R, Mistrík J, Dionne G F, Veis M and Ross C A 2016 Optical and magneto-optical behavior of cerium yttrium iron garnet thin films at wavelengths of 200–1770nm *Sci. Rep.* **6** 23640
[23] Stancil D D and Prabhakar A 2009 *Spin Waves-Theory and Applications* (New York: Springer)
[24] Pierce D T and Spicer W E 1972 Electronic structure of amorphous Si from photoemission and optical studies *Phys. Rev.* B **5** 307
[25] Gao L, Lemarchand F and Lequime M 2012 Exploitation of multiple incidences spectrometric measurements for thin film reverse engineering *Opt. Express* **20** 15734–51
[26] Kato H, Matsushita T, Takayama A, Egawa M, Nishimura K and Inoue M 2003 Theoretical analysis of optical and magneto-optical properties of one-dimensional magnetophotonic crystals *J. Appl. Phys.* **93** 3906
[27] Yu Z, Wang Z and Fan S 2007 One-way total reflection with one-dimensional magneto-optical photonic crystals *Appl. Phys. Lett.* **90** 121133
[28] Stefanou N, Yannopapas V and Modinos A 1998 Heterostructures of photonic crystals: frequency bands and transmission coefficients *Comput. Phys. Commun.* **113** 49–77

[29] Stefanou N, Yannopapas V and Modinos A 2000 MULTEM 2: a new version of the program for transmission and band-structure calculations of photonic crystals *Comput. Phys. Commun.* **132** 189–96
[30] Stefanou N, Karathanos V and Modinos A 1992 Scattering of electromagnetic waves by periodic structures *J. Phys.: Condens. Matter* **4** 7389
[31] Pendry J 1974 *Low Energy Electron Diffraction: The Theory and Its Application to Determination of Surface Structure* (New York: Academic)
[32] Katsidis C C and Siapkas D I 2002 General transfer-matrix method for optical multilayer systems with coherent, partially coherent, and incoherent interference *Appl. Opt.* **41** 3978–87
[33] Centurioni E 2005 Generalized matrix method for calculation of internal light energy flux in mixed coherent and incoherent multilayers *Appl. Opt.* **44** 7532–9
[34] Markoš P and Soukoulis C M 2008 *Wave Propagation: From Electrons to Photonic Crystals and Left-Handed Materials* (Princeton, NJ: Princeton University Press)
[35] Luque-Raigon J M, Halme J, Miguez H and Lozano G 2013 Symmetry analysis of the numerical instabilities in the transfer-matrix method *J. Opt.* **15** 125719
[36] Ko D Y K and Inkson J C 1988 Matrix method for tunneling heterostructures: resonant tunneling in multilayer system *Phys. Rev.* B **38** 9945